INTERNATIONAL JOURNAL FOR NUMERICAL AND ANALYTICAL METHODS IN GEOMECHANICS
Int. J. Numer. Anal. Meth. Geomech., **23**, 1535–1557 (1999)

AN ELASTOPLASTIC ANALYSIS OF NON-ISOTHERMAL CONSOLIDATION

H. ZHANG[1], M. BAI[2,*], Y. ABOUSLEIMAN[3] AND J.-C. ROEGIERS[2]

[1] *Dept. of Mechanical Engineering, University of Petroleum, Beijing, People's Republic of China*
[2] *Rock Mechanics Institute, University of Oklahoma, Norman, OK 73019, U.S.A.*
[3] *Dept. of Civil Engineering, School of Engineering and Architecture, Lebanese American University, Byblos, Lebanon*

SUMMARY

A thermoporoelastoplastic analysis of a one-dimensional column consolidation is presented to identify the critical parameters that may influence the processes involved in coupled fluid flow, heat flow, and rock deformation. In comparing with the usual thermoporoelastic approach, the present study shows that 'non-linear' elastoplasticity may replicate certain porous media responses which cannot be reproduced by a linear elastic evaluation. These responses are: (a) Mandel's effect[1] in a one-dimensional geometry, (b) consolidation occurring at critical porosity, and (c) cataclastic pressure and temperature changes within plastic zones. Copyright © 1999 John Wiley & Sons, Ltd.

KEY WORDS: thermoporoelastoplasticity; consolidation; Mandel effect

INTRODUCTION

In analysing coupled phenomena, embedded complexities can be reflected in numerous aspects. Process complexities may involve interactive and simultaneous fluid and heat flow, rock deformation, and chemical reactions. Constitutive complexities, on the other hand, may imply the subtle transition between linear and non-linear relationships. Finally, material complexities may indicate the structural multiplicities within the 'grey' areas of elastic and non-elastic ranges. As a result of our analytical, numerical and experimental limitations, the complexities have always been either (a) simplified into the isolated single or dual processes, (b) confined to monotonic linear system, or (c) envisioned as homogeneous or bi-substance but purely elastic media. Under such circumstances, any addition of complexities to the simulation tends to show visible improvement over the physical characterization of a complicated system because single process occurring in a linear elastic medium rarely represents a 'true' phenomenon.

When Biot[2] proposed the formulation of the three-dimensional consolidation (known as poroelasticity) based on a phenomenological one-dimensional consolidation concept suggested by Terzaghi,[3] the simulated porous media were meant to be linear and elastic. However, Biot's poroelasticity has been since extended beyond the linear elastic scopes to encompass more general mechanisms such as non-linear poroelasticity,[4] poroplasticity,[5,6] and thermoporoelasticity.[7,8] Even though the non-linearities might introduce additional complications in the solution procedures whilst the thermal coupling would bring extra equations to solve, the porous media in

*Correspondence to: M. Bai, Rock Mechanics Institute, The University of Oklahoma, Norman, OK 73019, U.S.A.

CCC 0363–9061/99/131535–23$17·50

Received 24 December 1997
Revised 31 August 1998

these cases are confined to the elastic behaviour. The necessity of using plasticity theory can be warranted when the poroelastic material is subjected to the external loading which exceeds the elastic limit.

It is not the intent of the present study to tackle various complexities comprehensively. Instead, this paper examines merely a one-dimensional consolidation scenario for a porous elastoplastic medium under non-isothermal conditions, in which the analysis of influential factors related to the material behaviour, such as hardening in plastic region, is the focus of the discussion. Transient development of the induced solid deformation is governed by the magnitudes of both external load as well as the elastic limit of the porous medium, which controls the evolution of plastic zones. For simplicity, the constitutive principle is represented by a bi-linear elastoplastic strain–stress relationship. It should be emphasized in the stress–strain relationship that unloading is not considered. Based on this scenario, evaluation of residual plastic strain is not required. Some unusual modelling results such as Mandel's effect,[1] which has not been observed in the one-dimensional scenarios, identify the significant influences of the plastic deformation on the variations of displacement, pressure and temperature. They are radically different from a thermoporoelastic approach alone.

MATHEMATICAL FORMULATION AND NUMERICAL SCHEME

A one-dimensional consolidation scenario, as schematically shown in Figure 1, is reexamined. It is assumed that the laterally confined porous column with the height h is positioned over a rigid, impermeable, and adiabatic base. A load, F_0, applied instantaneously at the top of the column ($x = 0$), results in the consolidation of the column, along with the dissipation of pore pressure and temperature from the top, as shown in Figure 1. As time elapses, the induced elastic strain becomes progressively larger until it exceeds the elastic limit, then part of the column turns into plastic material. The transient deformation enables the whole column to turn into the plastic stage at certain time.

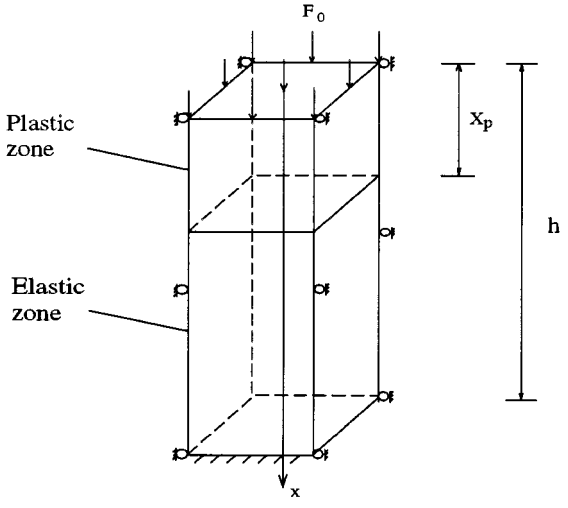

Figure 1. Schematic 1-D column

For such a problem, the compressive column is in a three-dimensional state, but can be simplified geometrically as a one-dimensional case. The equivalent effective stress, considering the stress coupling due to the compression of solid grains, interstitial pore pressure, and variations of fluid as well as solid temperatures, may be expressed as

$$\sigma_{eq} = \sigma_x + \alpha p + \beta T \tag{1}$$

where σ_x is the uniaxial stress, p is the pressure, T is the temperature, α is Biot's coefficient, which is defined as

$$\alpha = 1 - \frac{K}{K_s} \tag{2}$$

K and K_s are the bulk moduli of porous media and solid grains, respectively, and

$$K_s = \frac{E}{3(1-2v)} \tag{3}$$

E is the elastic modulus, v is Poisson's ratio, β is the thermal expansion factor and $\beta = \alpha_h(3\lambda + 2G)$, α_h is the thermal expansion coefficient, λ and G are Lamé's constants.

A fully coupled thermoporoelastic formulation may be described as[8]

$$\eta \frac{\partial^2 u}{\partial x^2} = \alpha \frac{\partial p}{\partial x} + \beta \frac{\partial T}{\partial x} \tag{4}$$

$$\frac{k}{\mu} \frac{\partial^2 p}{\partial x^2} = \alpha^* \frac{\partial p}{\partial t} + \alpha \frac{\partial^2 u}{\partial x \partial t} - \alpha_h \frac{\partial T}{\partial t} \tag{5}$$

$$K^* \frac{\partial^2 T}{\partial x^2} = \beta T_0 \frac{\partial^2 u}{\partial x \partial t} + s^* \frac{\partial T}{\partial t} \tag{6}$$

where u is the displacement, $\eta = \lambda + 2G$, k is the fluid permeability, μ is the fluid dynamic viscosity, α^* is the lumped compressibility, which is expressed as

$$\alpha = \frac{n}{K_f} + \frac{1-n}{K_s} \tag{7}$$

K_f is the fluid bulk modulus, n is the porosity, K^* is the thermal conductivity, s^* is the lumped intrinsic heat capacity, and T_0 is the reference temperature.

The boundary and initial conditions can be given as

$$\frac{\partial u(0,t)}{\partial x} = \frac{-F_0}{\eta}, \quad p(0,t) = T(0,t) = 0$$

$$u(h,t) = 0, \quad \frac{\partial p(h,t)}{\partial x} = \frac{\partial T(h,t)}{\partial x} = 0$$

$$p(x,0) = p_0, \quad T(x,0) = T_0 \tag{8}$$

where p_0 and T_0 are the initial pressure and temperature, and theoretically they should be calculated through solving static undrained as well as adiabatic systems, respectively.[2,9]

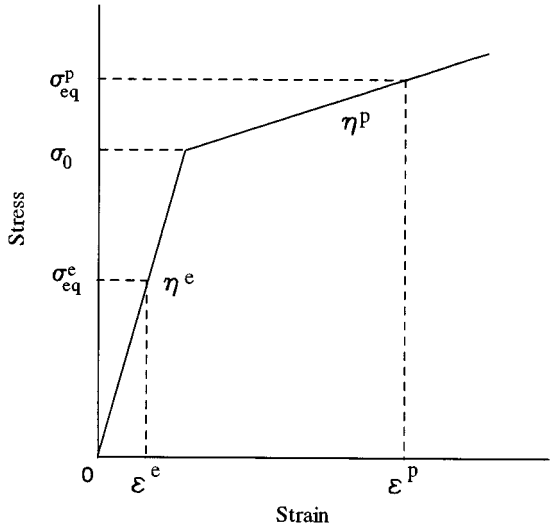

Figure 2. Bilinear stress–strain relationship

In general, the stress–strain behaviour of rock is non-linear, especially in the case where external load exceeds the elastic limit of material and the material becomes plastic. For simplicity, however, a bilinear stress–strain relationship is assumed, as shown in Figure 2. In addition, the Tresca yield criterion is used to determine the elastic–plastic transition of the column.

The yield condition can be expressed as

$$\sigma_{eq} + \sigma_0 = 0 \tag{9}$$

where σ_0 is the yield stress of column material.

Because the maximum load is imposed at the top of column, which accompanies by the fluid drainage, the material yield will be initiated at that location; and, as time elapses, the induced plastic zone propagates downward. With reference to Figure 2, the strains in the elastic portion (with superscript 'e') and the plastic portion (with superscript 'p') can be defined as

$$\begin{aligned} \varepsilon^{e} &= \frac{\sigma_{eq}}{\eta^{e}} \\ \varepsilon^{p} &= \frac{\sigma_{eq} + \sigma_0}{\eta^{p}} - \frac{\sigma_0}{\eta^{e}} \end{aligned} \tag{10}$$

where η^{e} and η^{p} are the elastic modulus and the linear hardening modulus of the material, respectively.

Integrating equation (4) with respect to x, and substituting the result into equations (5) and (6), governing equations (4)–(6) are modified into the following form for the elastic zone:

$$\frac{\partial u^{e}}{\partial x} = \frac{-F_0 + \alpha p^{e} + \beta^{e} T^{e}}{\eta^{e}}$$

$$\frac{\partial^2 p^{\mathrm{e}}}{\partial x^2} = g^{\mathrm{e}}_{11}\frac{\partial p^{\mathrm{e}}}{\partial t} + g^{\mathrm{e}}_{12}\frac{\partial T^{\mathrm{e}}}{\partial t}$$
$$\frac{\partial^2 T^{\mathrm{e}}}{\partial x^2} = g^{\mathrm{e}}_{21}\frac{\partial p^{\mathrm{e}}}{\partial t} + g^{\mathrm{e}}_{22}\frac{\partial T^{\mathrm{e}}}{\partial t} \tag{11}$$

where

$$\begin{aligned} g^{\mathrm{e}}_{11} &= \frac{\mu}{k}\left(\alpha^* + \frac{\alpha^2}{\eta^{\mathrm{e}}}\right) \\ g^{\mathrm{e}}_{12} &= \frac{\mu}{k}\left(\frac{\alpha\beta^{\mathrm{e}}}{\eta^{\mathrm{e}}} - \alpha_{\mathrm{h}}\right) \\ g^{\mathrm{e}}_{21} &= \frac{\alpha\beta^{\mathrm{e}} T_0}{K^*\eta^{\mathrm{e}}} \\ g^{\mathrm{e}}_{22} &= \frac{1}{K^*}\left(s^* + \frac{(\beta^{\mathrm{e}})^2 T_0}{\eta^{\mathrm{e}}}\right) \end{aligned} \tag{12}$$

and where the superscript 'e' represents the elastic properties.

Similarly, the modified governing equations for the plastic zone can be written as

$$\frac{\partial u^{\mathrm{p}}}{\partial x} = \frac{-F_0 + \alpha p^{\mathrm{p}} + \beta^{\mathrm{p}} T^{\mathrm{p}} + \sigma_0}{\eta^{\mathrm{p}}} - \frac{\sigma_0}{\eta^{e}}$$
$$\frac{\partial^2 p^{\mathrm{p}}}{\partial x^2} = g^{\mathrm{p}}_{11}\frac{\partial p^{\mathrm{p}}}{\partial t} + g^{\mathrm{p}}_{12}\frac{\partial T^{\mathrm{p}}}{\partial t} \tag{13}$$
$$\frac{\partial^2 T^{\mathrm{p}}}{\partial x^2} = g^{\mathrm{p}}_{21}\frac{\partial p^{\mathrm{p}}}{\partial t} + g^{\mathrm{p}}_{22}\frac{\partial T^{\mathrm{p}}}{\partial t}$$

where

$$\begin{aligned} g^{\mathrm{p}}_{11} &= \frac{\mu}{k}\left(\alpha^* + \frac{\alpha^2}{\eta^{\mathrm{p}}}\right) \\ g^{\mathrm{p}}_{12} &= \frac{\mu}{k}\left(\frac{\alpha\beta^{\mathrm{p}}}{\eta^{\mathrm{p}}} - \alpha_{\mathrm{h}}\right) \\ g^{\mathrm{p}}_{21} &= \frac{\alpha\beta^{\mathrm{p}} T_0}{K^*\eta^{\mathrm{p}}} \\ g^{\mathrm{p}}_{22} &= \frac{1}{K^*}\left(s^* + \frac{(\beta^{\mathrm{p}})^2 T_0}{\eta^{\mathrm{p}}}\right) \end{aligned} \tag{14}$$

and where the superscript 'p' represents the plastic properties.

The continuity conditions must be satisfied at the interface between the elastic and the plastic zones, i.e.

$$\begin{aligned} u^{\mathrm{e}}|_{x=x_{\mathrm{p}}} &= u^{\mathrm{p}}|_{x=x_{\mathrm{p}}} \\ p^{\mathrm{e}}|_{x=x_{\mathrm{p}}} &= p^{\mathrm{p}}|_{x=x_{\mathrm{p}}} \\ T^{\mathrm{e}}|_{x=x_{\mathrm{p}}} &= T^{\mathrm{p}}|_{x=x_{\mathrm{p}}} \end{aligned} \tag{15}$$

As a result of the difficulty of deriving the closed-form analytical solutions for the above equations, the explicit finite difference method was employed. Therefore, equations (11) and (13) can be discretized as

$$\begin{aligned}
&\frac{p^{\mathrm{e}}_{i,j+1} - 2p^{\mathrm{e}}_{i,j} + p^{\mathrm{e}}_{i,j-1}}{\Delta x^2} = g^{\mathrm{e}}_{11}\frac{p^{\mathrm{e}}_{i+1,j} - p^{\mathrm{e}}_{i,j}}{\Delta t} + g^{\mathrm{e}}_{12}\frac{T^{\mathrm{e}}_{i+1,j} - T^{\mathrm{e}}_{i,j}}{\Delta t}\\
&\frac{T^{\mathrm{e}}_{i,j+1} - 2T^{\mathrm{e}}_{i,j} + T^{\mathrm{e}}_{i,j-1}}{\Delta x^2} = g^{\mathrm{e}}_{21}\frac{p^{\mathrm{e}}_{i+1,j} - p^{\mathrm{e}}_{i,j}}{\Delta t} + g^{\mathrm{e}}_{22}\frac{T^{\mathrm{e}}_{i+1,j} - T^{\mathrm{e}}_{i,j}}{\Delta t}\\
&\frac{u^{\mathrm{e}}_{i,j+1} - u^{\mathrm{e}}_{i,j}}{\Delta x} = \frac{-F_0 + \alpha p^{\mathrm{e}}_{i,j} + \beta^{\mathrm{e}} T^{\mathrm{e}}_{i,j}}{\eta^{\mathrm{e}}}
\end{aligned} \tag{16}$$

and

$$\begin{aligned}
&\frac{p^{p}_{i,j+1} - 2p^{p}_{i,j} + p^{p}_{i,j-1}}{\Delta x^2} = g^{p}_{11}\frac{p^{p}_{i+1,j} - p^{p}_{i,j}}{\Delta t} + g^{p}_{12}\frac{T^{p}_{i+1,j} - T^{p}_{i,j}}{\Delta t}\\
&\frac{T^{p}_{i,j+1} - 2T^{p}_{i,j} + T^{p}_{i,j-1}}{\Delta x^2} = g^{p}_{21}\frac{p^{p}_{i+1,j} - p^{p}_{i,j}}{\Delta t} + g^{p}_{22}\frac{T^{p}_{i+1,j} - T^{p}_{i,j}}{\Delta t}\\
&\frac{u^{p}_{i,j+1} - u^{p}_{i,j}}{\Delta x} = \frac{-F_0 + \alpha p^{p}_{i,j} + \beta^{p} T^{p}_{i,j} + \sigma_0}{\eta^{p}} - \frac{\sigma_0}{\eta^{\mathrm{e}}}
\end{aligned} \tag{17}$$

The boundary and initial conditions can be written as

$$\begin{aligned}
&p_{i,1} = 0, \quad T_{i,1} = 0 \quad \text{at } x = 0\\
&p_{i,j+1} = p_{i,j}, \quad T_{i,j+1} = T_{i,j}, \quad u_{i,j+1} = 0 \quad \text{at } x = h\\
&p_{1,j} = p_0, \quad T_{1,j} = T_0 \quad \text{at } t = 0
\end{aligned} \tag{18}$$

where i, j are increment numbers of differential mesh for time and depth, respectively.

SENSITIVITY ANALYSES

The sensitivity analyses are aimed at determining the variations of material properties that affect the changes in displacement, pressure and temperature. The particular objective is to identify the difference between the thermoporoelastic and the thermoporoelastoplastic solutions. The selected parameter ranges, with respect to the hydraulic, thermal, mechanical and geometrical categories, are listed in Table I, while the pressure p, temperature T, displacement u and plastic zone depth x_{p} are normalized with respect to their initial or maximum values. The dimensionless time is chosen in the normal manner[8] as

$$\tau = \frac{c_v t}{h^2} \tag{19}$$

where c_v is the coefficient of consolidation, and h is the height of the consolidating column.

The point of interest is selected at 6 m from the top of the column. The material at this location is expected to change from the initial elastic state to the plastic state as time increases. In the following figures, notation of 'elastic' solution implies the thermoporoelastic one,[8] while that of 'elastoplastic' solution means the thermoporoelastoplastic one. All parametric units can be referred to Table I, but are omitted in the following for brevity. Porosity $n = 0{\cdot}4$ is used for Figures 3–5. Unless specified, the plastic module $E^{\mathrm{p}} = 5 \times 10^8$ is used for most cases.

Table I. Selected thermoporoelastoplastic parametric ranges

Category	Symbol	Value range	Unit
Hydraulic	k	3×10^{-10}–10^{-9}	m^2
	μ	20	kg/(m, h)
	n	0·01–0·4	—
	p_0	10^4	Pa
Thermal	α_f	10^{-5}	1/°C
	α_s	10^{-6}	1/°C
	K_f^*	100–5000	J/(m, h, °C)
	K_s^*	10–500	J/(m, h, °C)
	ρ_f	1000	kg/m^3
	ρ_s	2000	kg/m^3
	c_f	100–1000	J/(kg, °C)
	c_s	20–500	J/(kg, °C)
	T_0	100	°C
Mechanical	α	0·9	—
	ν^e	0·25	—
	ν^p	0·45	—
	E^e	5×10^9	Pa
	E^p	5×10^8–5×10^9	Pa
	K_f	5×10^9	Pa
	K_s	2×10^{10}	Pa
	F_0	5×10^6	Pa
	σ_0	1×10^6	Pa
Geometric	h	100	m
	x	6	m

Note: Superscript e-Elastic, p-Plastic

In the sensitivity analysis, only one parameter is allowed to change while all other parameters are fixed. This manipulation may not represent the chain effect that may occur in the reality. As a result, the outcomes show the limited influences for each particular parameter under investigation.

From the bilinear stress–strain relationship shown in Figure 2, it is known that the deformation is more significant after the material yields; this in turn results in greater pore pressure variations. As shown in Figure 3, significant changes in pore pressure can be identified as the elastic modulus drops from the elastic state to the progressively less stiffer state. One interesting observation is that the pore pressure is larger than the original magnitude when the elastic modulus is one order of magnitude lesser than that in the elastic state. This so-called Mandel effect,[1] i.e. an increase of the pore pressure soon after the initial loading, is observed previously only in the two dimensional geometry where the fluid escape is slower than the transmitted elastic deformation after the loading, thus creating the higher pressure value. The pore pressure will drop below the original magnitude after elapse of time during fluid drainage. This one-dimensional Mandel effect[1] seems to relate to larger plastic deformation because the rate of pore pressure dissipation may mismatch the rate of the larger plastic deformations at earlier times. In contrast, however, variations of the elastic and plastic moduli show almost no impact on the changes in temperature (Figure 4). For

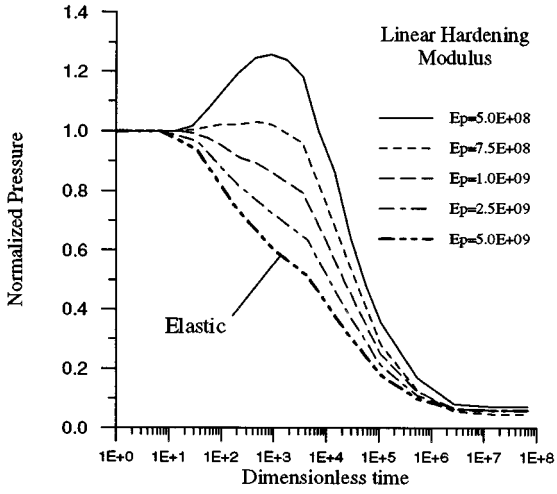

Figure 3. Temporal pressure for various moduli

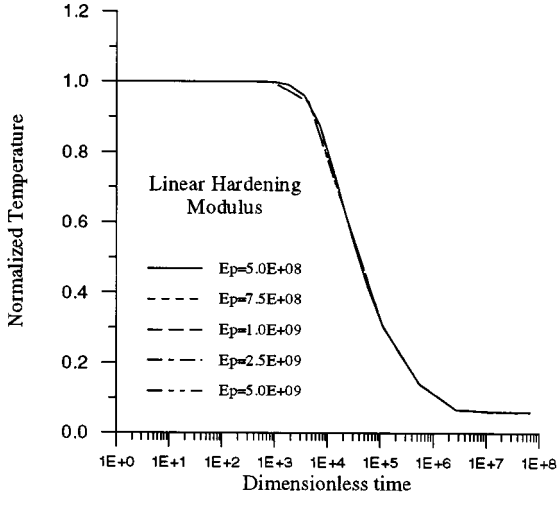

Figure 4. Temporal temperature for various moduli

the displacements, Figure 5 indicates that the approximate proportionality exists between the elastic moduli and the displacements.

The variations of column porosity demonstrate the significant influence over the pore pressure changes, as illustrated in Figure 6. It may be observed that the pore pressure dissipation is further delayed as the porosity increases, because the larger storage capacity allows slower fluid drainage. As noted in Figure 6, the one-dimensional Mandel effect[1] starts to appear when the porosity

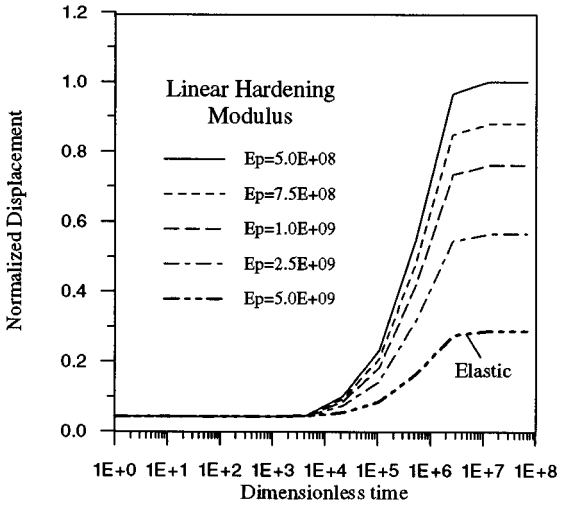

Figure 5. Temporal displacement for various moduli

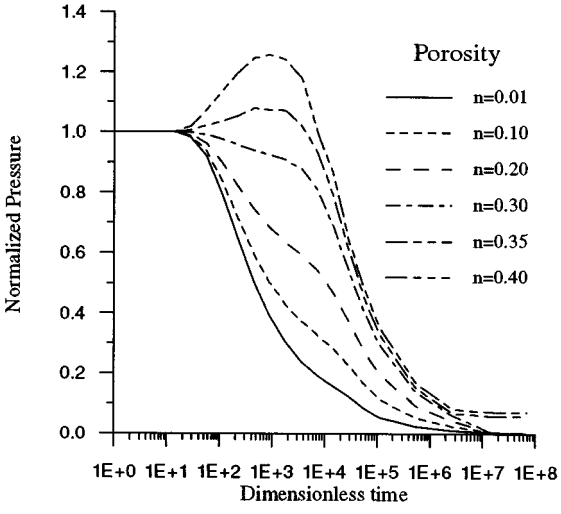

Figure 6. Temporal pressure for various porosities

exceeds 0·35. The comparison of temporal pressures for elastic,[8] and elastoplastic (this paper) using larger ($n = 0{\cdot}4$) and smaller ($n = 0{\cdot}01$) porosities is shown in Figure 7. It is seen that significant differences between the two different constitutive relations result from the larger porosity only. The most significant difference occurs for the elastoplastic material when the porosity varies from the smaller to the larger values. Deviating from the impact of elastic modulus on the temperature changes, the porosity variations indeed incurs noticeable changes in the pore

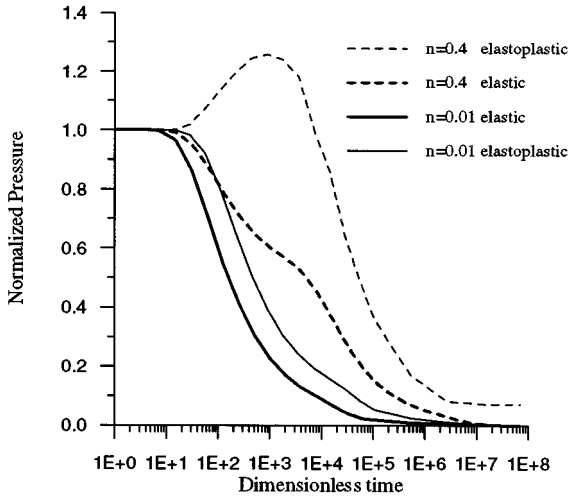

Figure 7. Comparison between elastic and elastoplastic cases

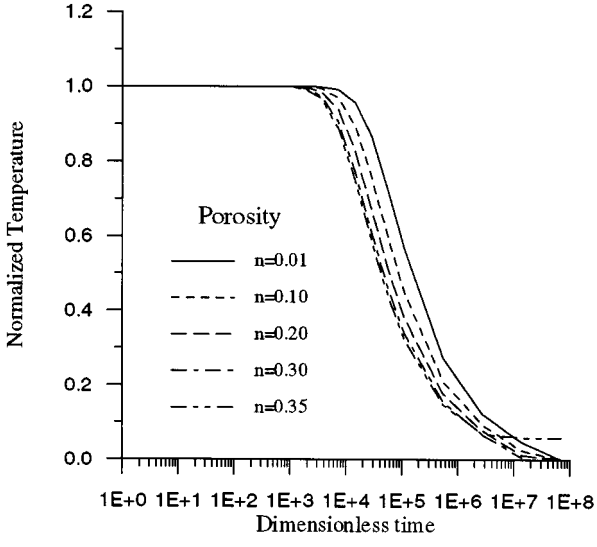

Figure 8. Temporal temperature for various porosities

pressure, as shown in Figure 8. However, the changes are not so significant as to introduce the Mandel effect.[1]

The relationship between the evolution of the plastic zone and porosity variations is depicted in Figure 9. It is seen that the column becomes total plastic suddenly instead of asymptotically except when the porosity is 0·3. In general, larger porosity prolongs the pore pressure dissipation,

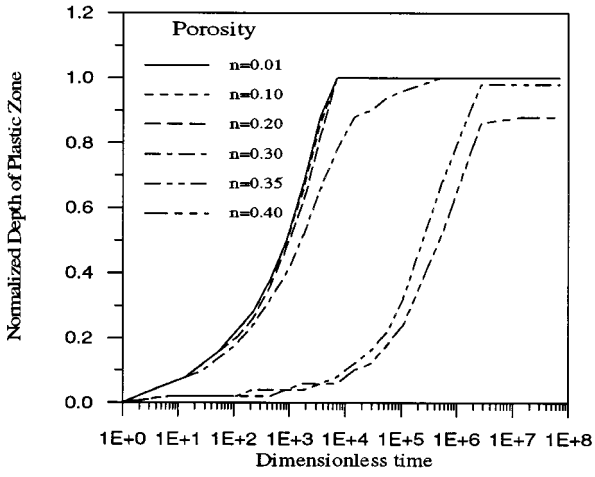

Figure 9. Plastic zone for various porosities

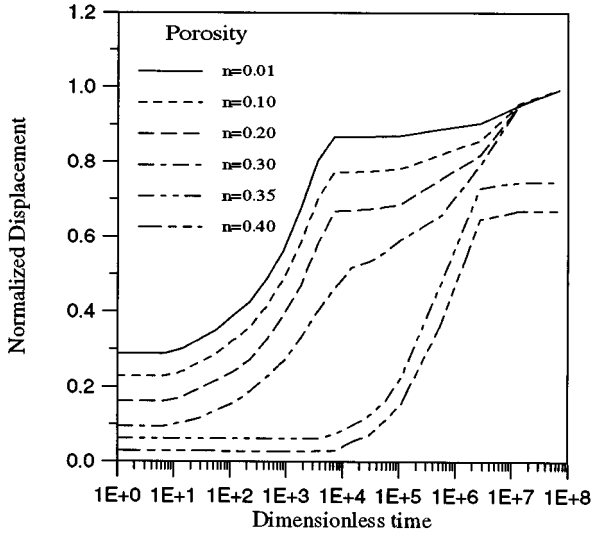

Figure 10. Temporal displacement for various porosities

thus delays the development of the plastic zone. In view of the displacements, the porosity variations seem to generate quite different temporal displacement profiles (Figure 10). Greater initial consolidation appears to be associated with smaller porosity. The displacement profile looks rather irregular, with quite radical changes occurring at the initial stage. The comparison of the displacements between the elastic and elastoplastic solutions for larger and smaller porosities, as shown in Figure 11, indicates that the irregularity in the temporal displacement is indeed

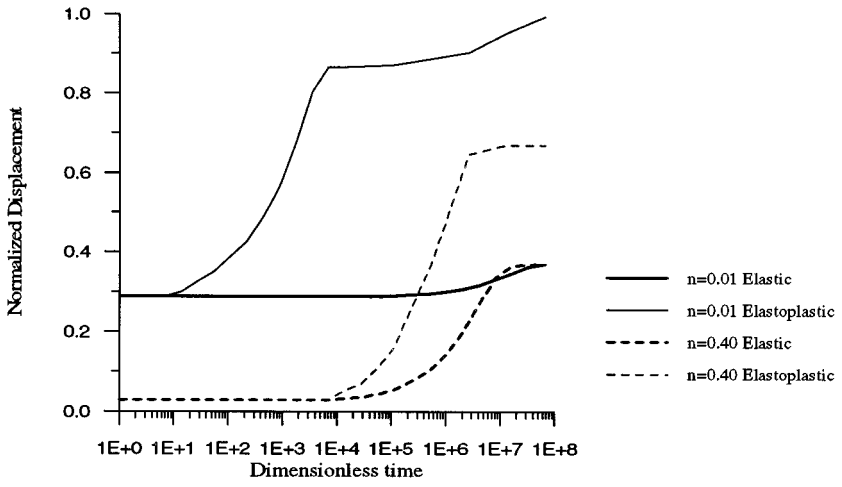

Figure 11. Comparison between elastic and elastoplastic cases

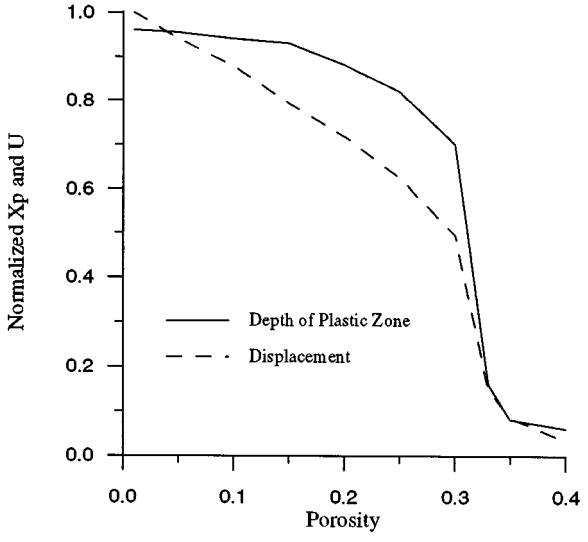

Figure 12. Plastic zone and displacement versus porosity

attributed to the elastoplastic deformation for the smaller porosities. By further examining the elastoplastic case when $n = 0{\cdot}01$, the sudden change of displacement at the dimensionless time $\tau = 8000$ reflects the transition when the material changes from the partial plastic state to the total plastic state. In the later stage, the rate of displacement reduces before the material shows the delayed hardening characteristics. Compared with the elastic deformation for the same

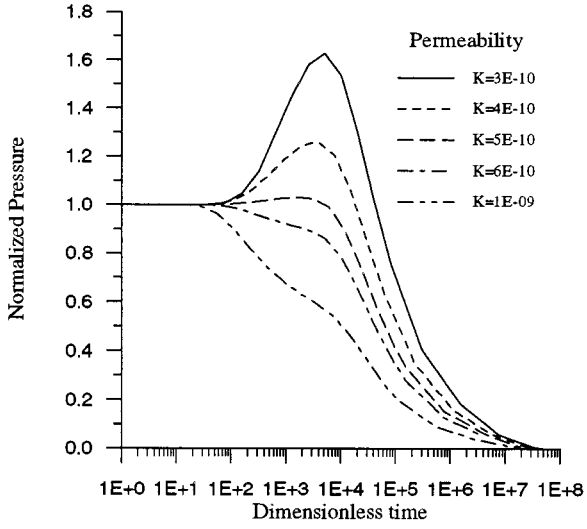

Figure 13. Temporal pressure for various permeabilities

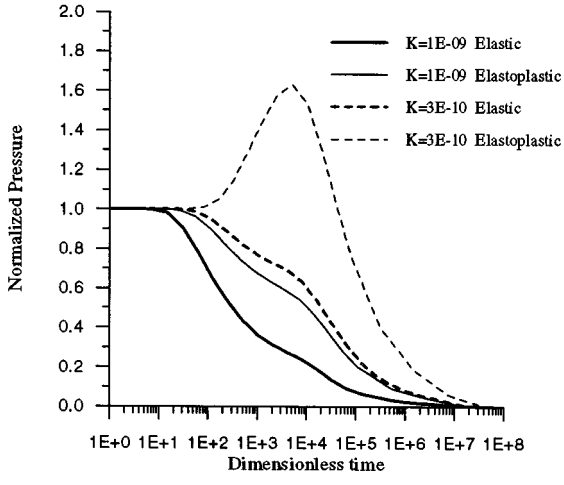

Figure 14. Comparison between elastic and elastoplastic cases

porosity, elastoplastic deformation is much more significant. In contrast, this difference is substantially reduced for the larger porosity case ($n = 0{\cdot}4$). Another observation is that the magnitude of porosity also controls the initial displacements. At the dimensionless time $\tau = 1 \times 10^6$, the correlation between the porosity and the depth of the plastic zone as well as the displacement is shown in Figure 12. It may be noted that the drastic displacement changes occur when the porosity varies from 0·3 to 0·35, while both depths of plastic zone and displacements are

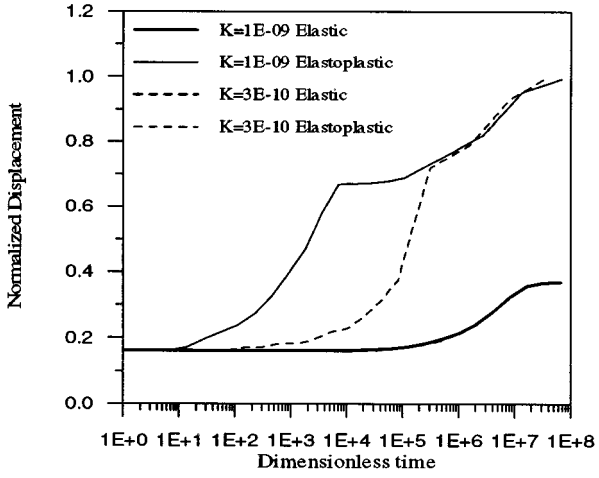

Figure 15. Comparison between elastic and elastoplastic cases

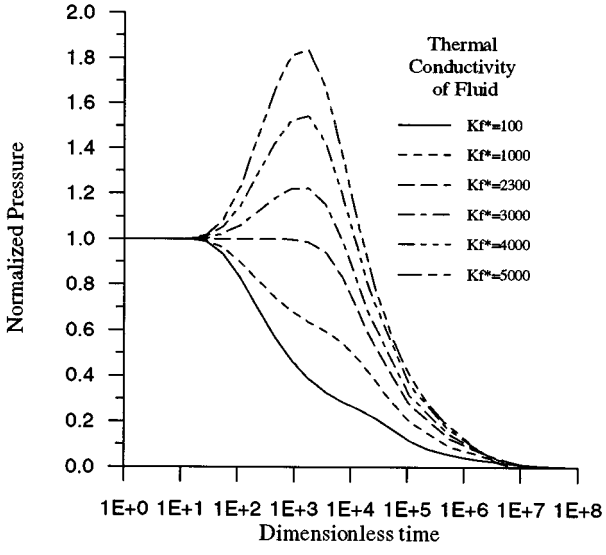

Figure 16. Temporal pressure for various fluid thermal conductivities

subjected to the significant magnification at the lower porosity range. In other words, larger deformations and plastic failure may be preventable for quite permeable porous media.

The temporal pressure development for various column permeabilities may follow the similar patterns as that for various elastic moduli (Figure 3), as shown in Figure 13, except that the Mandel effect[1] seems to be more manifested even for the lesser permeability changes. The comparison of pressure between the elastic and elastoplastic solutions for larger and smaller

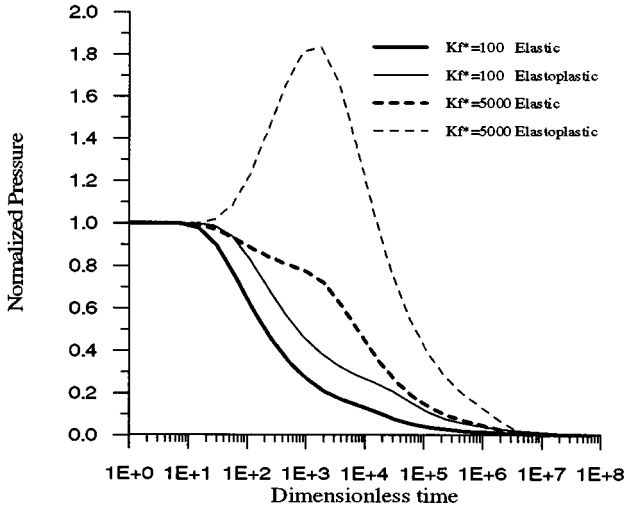

Figure 17. Comparison between elastic and elastoplastic cases

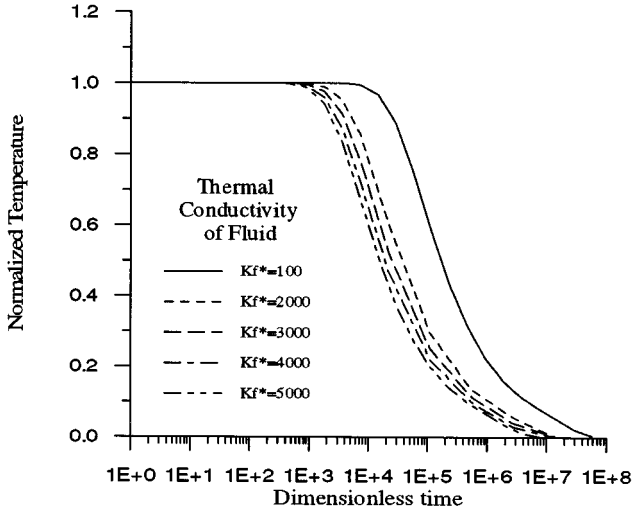

Figure 18. Temporal temperature for various fluid thermal conductivities

permeabilities is given in Figure 14. Indeed, the so-called Mandel effect[1] is associated with the elastoplastic case for the smaller permeability only, in which the lower permeable material, in general, leads to the generation of higher pore pressures, and, consequently, the moment of the initial pressure increase. The elastic and elastoplastic displacements for larger and smaller permeabilities are compared in Figure 15. It is of interest to note that there is no change in the displacements for the elastic solutions even though the permeabilities are different. However, for

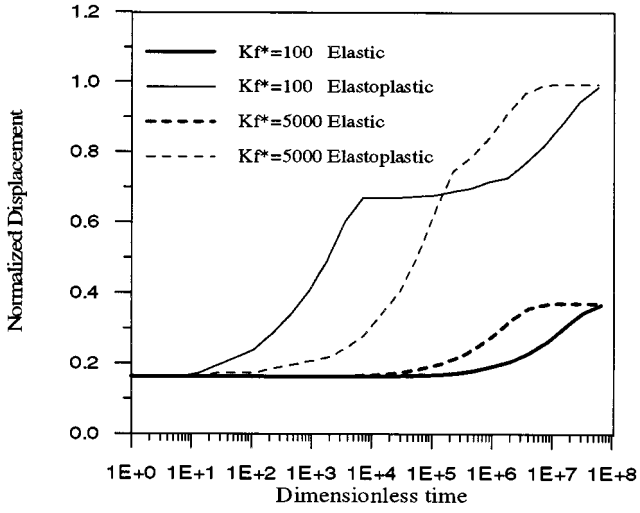

Figure 19. Comparison between elastic and elastoplastic cases

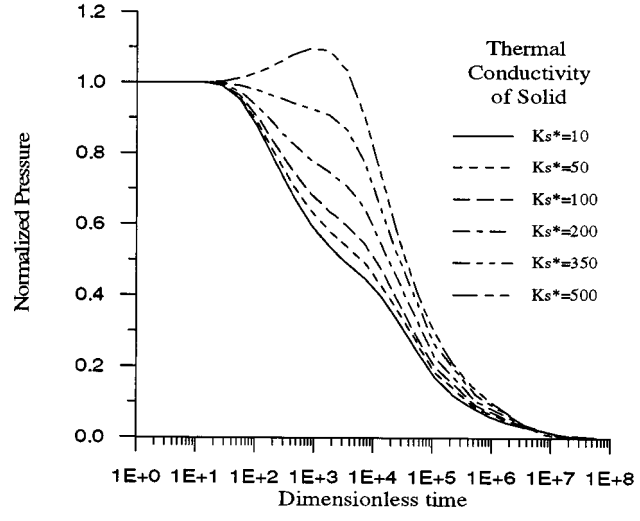

Figure 20. Temporal pressure for various solid thermal conductivities

the same change in permeabilities, the solutions for the elastoplastic cases show the noticeable difference in the displacements.

The changes in thermal properties, such as the thermal conductivity of the fluid, may result in significant modifications of the temporal pressure distributions, as depicted in Figure 16. In general, the higher the fluid thermal conductivity, the larger the difference that will result between

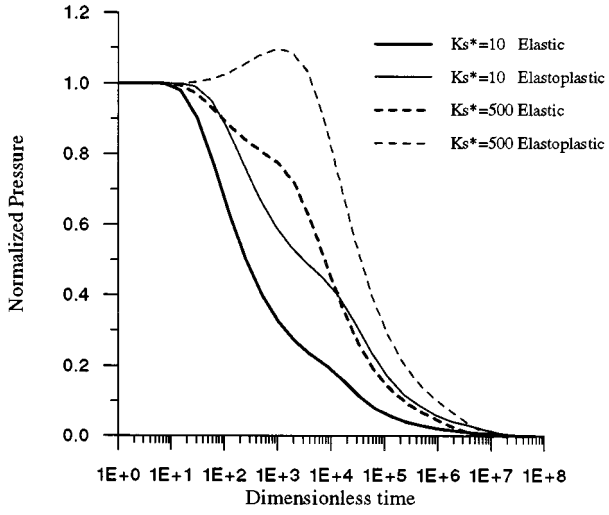

Figure 21. Comparison between elastic and elastoplastic cases

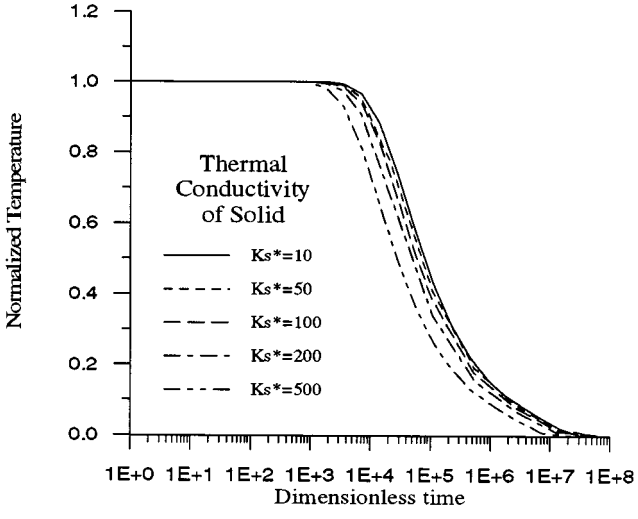

Figure 22. Temporal temperature for various solid thermal conductivities

the elastic and elastoplastic solutions, as indicated in Figure 17. The variations of the fluid thermal conductivity lead to more significant changes in the temporal temperature distributions (Figure 18). The larger conductivity, in general, promotes an earlier temperature dissipation. However, unlike in the temporal pressure distributions, no Mandel effect[1] can be identified in the temperature profiles. In other words, the temperature variations show less coupled effects with

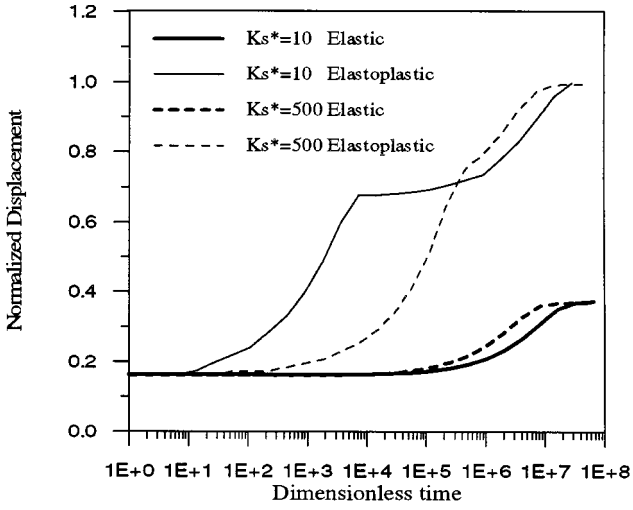

Figure 23. Comparison between elastic and elastoplastic cases

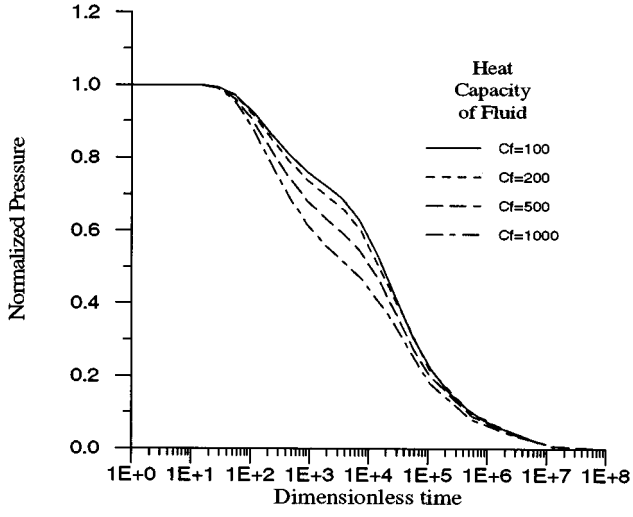

Figure 24. Temporal pressure for various fluid heat capacities

the changes in solid deformations; or, the temperatures show a more diffusive nature. The less significant effect of fluid thermal conductivity variations on the changes of displacements is described in Figure 19, but the difference in the result between the elastic and elastoplastic solutions remains substantial.

The changes of temporal pressures for various thermal conductivities of the solid show essentially similar trend as those from other parametric changes, as shown in Figure 20. However,

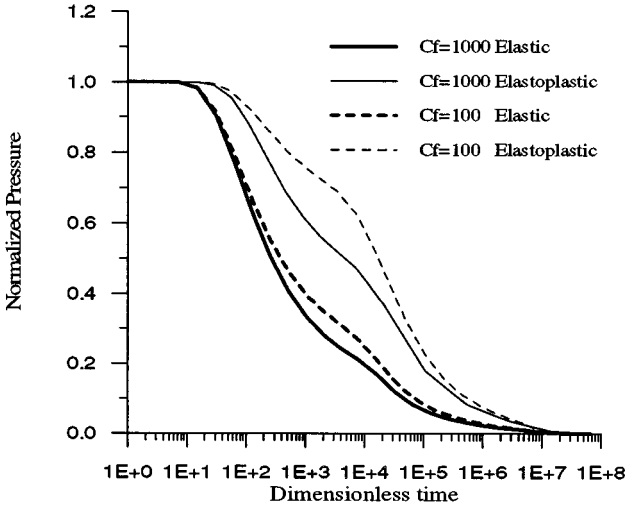

Figure 25. Comparison between elastic and elastoplastic cases

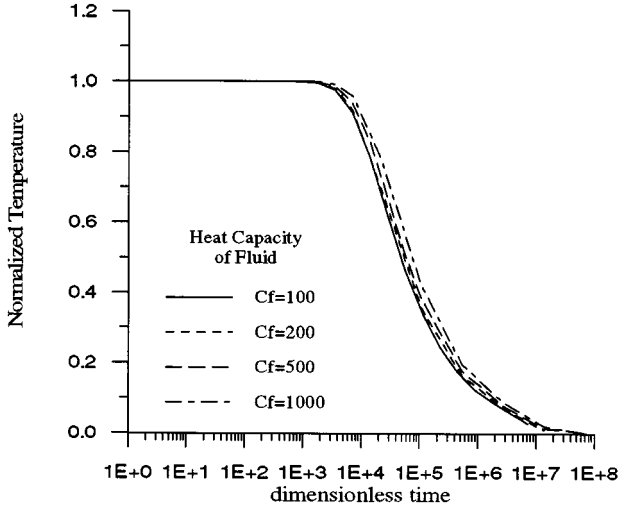

Figure 26. Temporal temperature for various fluid heat capacities

the Mandel effect[1] may be less obvious, so is the difference between the elastic and elastoplastic solutions (Figure 21), and the temperatures (Figure 22). Though, the difference in the displacements between the elastic and elastoplastic solutions maintains exceptionally large (Figure 23).

In view of thermal storage changes, Figure 24 indicates that the pressures are less likely affected by the changes in the fluid heat capacity. Unlike any other cases for the temporal pressures, no

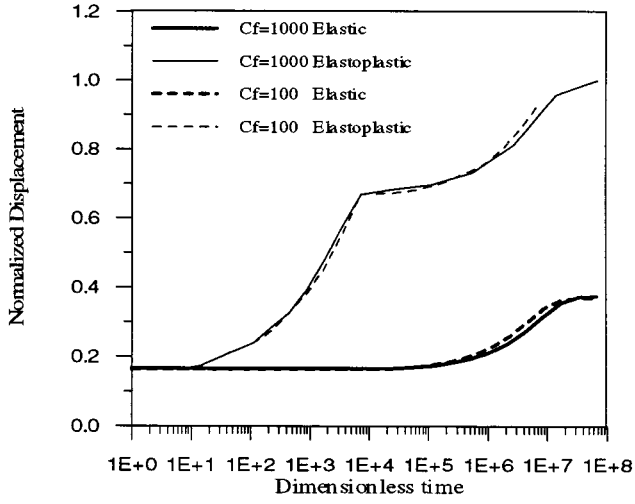

Figure 27. Comparison between elastic and elastoplastic cases

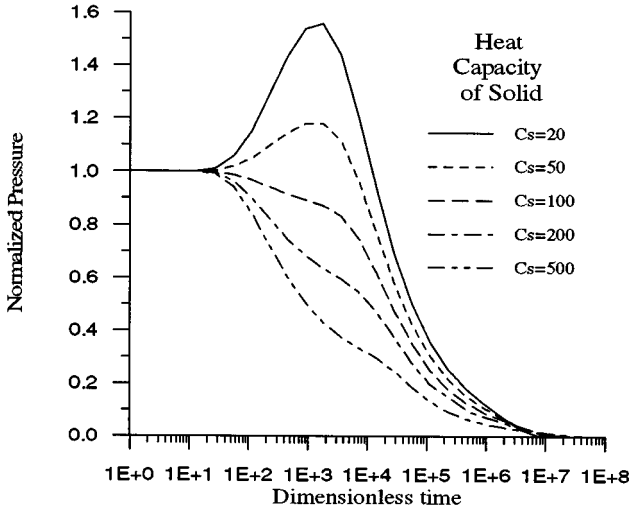

Figure 28. Temporal pressure for various solid heat capacities

Mandel effect[1] is visible. The elastic and elastoplastic solutions show the reduced disparities even with wide range fluctuation in the fluid heat capacity (Figure 25). The differences are further reduced to a minimum for distributions of temperatures (Figure 26), and displacements (Figure 27), except for the difference between the elastic and elastoplastic solutions for the latter case. However, the variations of pressures (Figures 28 and 29), temperatures (Figure 30) and displacements (Figure 31) restore the more significant differences with the variations in the heat

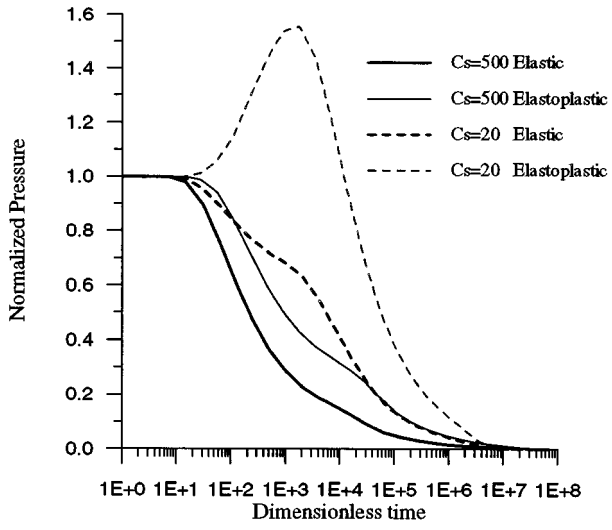

Figure 29. Comparison between elastic and elastoplastic cases

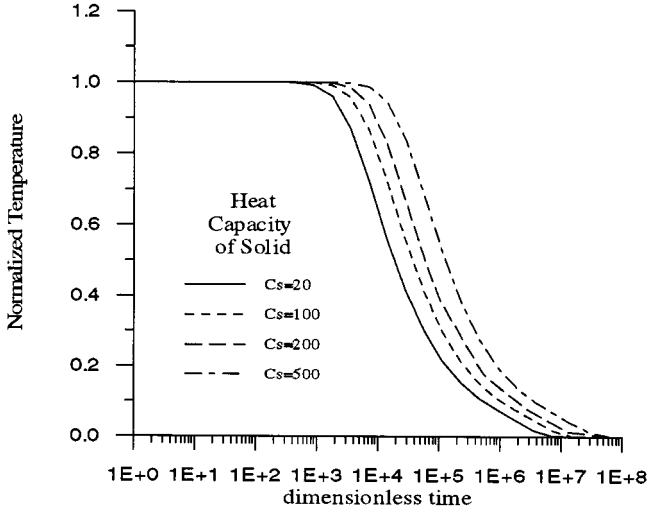

Figure 30. Temporal temperature for various solid heat capacities

capacity of the solid. In general, the larger solid heat capacity leads to earlier pressure and temperature dissipations, while plastic deformations with smaller solid heat capacity appear to contribute to the occurence of the Mandel effect,[1] as observed earlier. This contrast may reveal that the changes in the solid thermal properties may play a more important role than these in the fluid thermal properties in this thermoporoelastoplastic system.

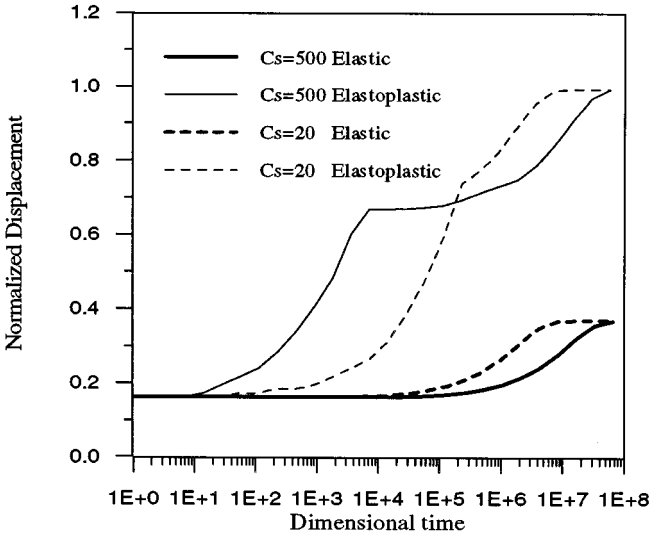

Figure 31. Comparison between elastic and elastoplastic cases

CONCLUSIONS

A thermoporoelastoplastic numerical solution is presented to investigate the one-dimensional consolidation column problem subjected to a non-isothermal environment. The most important finding of this study may be reflected in its identification of certain responses which cannot be replicated using the traditional thermoporoelastic approach. In the past, the so-called Mandel effect[1] was only observed in the two-dimensional domain simulation in which the geometry plays an essential role on the initial pressure increase. The Mandel effect[1] identified in the present 1-D study can be attributed mainly to the effect of large plastic deformations when other material parameters (e.g. hydraulic, thermal) fall within certain ranges. However, this Mandel effect[1] occurs only in the pore pressure variations. The temperature changes are primarily confined to the diffusion-dominated features. Significant differences are recognized between the elastic and elastoplastic solutions, in particular for the displacements. A critical porosity range seems to exist between 0·3 and 0·35. Outside this range, the calculated consolidation is either significantly large, or negligibly small. Except for the temperature dissipation, many distribution curves show variable slopes and radical changes, an obvious indication that the results are affected by the coupled multiple processes. The significant parameters identified in this analysis are: elastic and plastic modulii, porosity, permeability, thermal conductivity of the fluid, and thermal capacity of the solid.

ACKNOWLEDGEMENT

Support of the National Science Foundation/State/Industry under the S/IUCRC program and under the contract EEC-9209619, and financial support from the Chinese National Petroleum Cooperation (CNPC), are gratefully acknowledged.

REFERENCES

1. J. Mandel, 'Consolidation des sols', *Géotechnique*, **3,** 287–299 (1953).
2. M. A. Biot, 'General theory of three-dimensional consolidation', *J. Appl. Phys.*, **12,** 155–164 (1941).
3. K. Terzaghi, 'Die Berechnung der Durchassigkeitsziffer des Tones aus dem Verlauf der hydro-dynamischen Spannungsercheinungen', *Sitzungsber. Akad. Wiss. Wien Math-Naturwiss. Kl., Abt.*, 2A, **132,** 105 (1923).
4. C. S. Desai, T. Kuppusamy, D. C. Koutsoftas and R. Janardhanam, 'A one-dimensional finite element procedure for nonlinear consolidation', *Proc. 3rd Int. Conf. Num. Meth. Geomech.*, Aachen, pp. 1979, 143–148.
5. O. Coussy, 'A general theory of thermoporoelastoplasticity for saturated porous materials', *Transport in Porous Media*, **4**, 281–293 (1989).
6. Ph.A. Charlez, *Rock Mechanics, Vol. 1, Theoretical Fundamentals*, Technip, Paris, 1991.
7. D. W. Smith and J. R. Booker, 'Green's functions for a fully coupled thermoporoelastic material', *Int. J. Numer. Anal. Methods Geomech.*, **17,** 139–163 (1993).
8. M. Bai and Y. Abousleiman, 'Thermoporoelastic coupling with application to consolidation', *Int. J. Numer. Anal. Methods Geomech.*, **21**, 121–132 (1997).
9. J. Ghaboussi and E. L. Wilson, ('Flow of compressible fluid in porous elastic media', *Int. J. Num. Methods in Eng.*, **5,** 419–442 (1973).

